Natural ventilation performance of solar chimney with and without earth-air heat exchanger during transition seasons

Tianhe Long[a], Ningjing Zhao[a], Wuyan Li[b], Shen Wei[c], Yongcai Li[a,*], Jun Lu[a], Sheng Huang[a], Zhenyong Qiao[a]

[a]School of Civil Engineering, Chongqing University, Chongqing, 400045, China
[b]Department of Building Science, School of Architecture, Tsinghua University, Beijing, 100084, China
[c]The Bartlett School of Sustainable Construction, University College London (UCL), 1-19 Torrington Place, London, WC1E 7HB, United Kingdom

*Corresponding authors. Tel.: +86 2365123777; E-mail: yongcail85@163.com (Y. Li)

Abstract

This study experimentally investigates the natural ventilation performance of a solar chimney (SC) integrated with an earth-air heat exchanger (EAHE) during the transition seasons. The experiment was conducted in a comparative manner under three operating modes: Mode A: SC operating with EAHE with the window closed; Mode B: SC operating with an open window with the same opening area as the cross-sectional area of the EAHE pipe, with the EAHE closed; Mode C: the operating mechanism was the same as that of Mode B with the window opening area doubled. The results showed that 24 h of natural ventilation was achieved for the three operating modes. However, the nocturnal ventilation driving force for Mode A was the heating effect of the subsoil, while that for Modes B and C was the heat released from the thermal mass. The average daytime and nocturnal airflow rates for Modes A, B, and C were 209 m^3/h and 139 m^3/h, 286 m^3/h and 87 m^3/h, and 340 m^3/h and 80 m^3/h, respectively. The 24 h overall heating and cooling capacities of the EAHE for Mode A were 19474 kJ and 2179 kJ, respectively. The SCEAHE system had an advantage in preserving acceptable indoor thermal comfort with a diurnal indoor temperature variation in the range 19.7−22.7 °C.

Keywords: earth–air heat exchanger; solar chimney; buoyancy force; natural ventilation; indoor thermal environment.

1. Introduction

The world's energy consumption has grown tremendously over the past few decades, in which the building sector accounts for more than 20 % of the world's total energy usage [1, 2]. However, occupants in buildings with high air-tightness suffer from sick building syndrome (SBS) [3]. The ambient air temperature significantly deviates from the thermal comfort limits during the hot and cold weathers. Hence, an energy-consuming handling process for fresh air is necessary [4]. However, when the outdoor air conditions are temperate in the transition seasons, it is desirable to induce the fresh air directly into the indoor space using natural ventilation (NV). NV is a zero-carbon solution to alleviate the energy shortages, improve the indoor air quality, and reduce the greenhouse gas (GHG) emission [5–7].

Compared with mechanical ventilation systems, passive ventilation systems relying on buoyant pressure and/or wind pressure further reduce the energy consumption by fans. Solar chimneys (SCs) have been adopted as an effective method to enhance the buoyant pressure and promote the airflow [8, 9]. The concept of SCs is similar to that of the conventional chimneys, except for the transparent cover on its southward wall. This design enables more solar radiation to pass through this transparent cover to heat the air inside the chimney. Owing to the stack effect, the warmed air gets a stronger force to move upward and escape from the top of the chimney. This phenomenon induces sucking of cooler air from the outdoor environment from the bottom of the chimney [10, 11]. SC can be used directly for ventilation and cooling purposes when the external environmental conditions are within the comfort limits [12, 13]. Daytime ventilation, based on SC, during the summer is not desirable owing to the high external temperatures [14, 15]. In addition, it is not suitable for winter, as the outdoor temperatures are lower than the comfort zone temperature levels [16, 17]. Although SC can enhance the efficiency of natural ventilation and provide adequate ventilation rates [18], it does not cool the incoming outdoor air, which can lead to discomfort when the outdoor temperature is high. Research indicates that an extremely high ventilation rate

is required for ventilating the indoor environment of a building because of the low cooling potential of the SC during hot weather [19]. Therefore, SCs are generally considered suitable for temperate climate zones or transition seasons. To improve the indoor thermal comfort further, coupling SC with other systems is advised to enhance its performance. An option is to couple the SC with earth-to-air heat exchangers (EAHE), which combine two renewable energy sources (solar and geothermal energies), and operate without carbon emissions [20, 21].

EAHE is a shallow geothermal utilisation system that uses air from the external environment as the working fluid to provide fresh air and cooling/heating capacity directly to the building [22]. The EAHEs consist of buried pipes, through which the outdoor air is transported using a fan. The buried pipes acting as heat exchangers are buried at a certain depth, where the climatic changes rarely influence the soil temperature. The induced air is pre-cooled/pre-heated by the surrounding soil in summer/winter. The current research interests focus primarily on the evaluation/improvement of cooling and heating potentials of EAHEs in summer and winter [23−26]. Khabbaz et al. [27] reported that the EAHE is a suitable semi-passive system for air refreshment, as the recorded outlet air temperature was quasi-constant at 25 °C, even though the outside temperature reached more than 40 °C, through summer monitoring. Li et al. [28, 29] experimentally verified the feasibility of EAHE combined with a heat recovery unit (HRU) as an independent heat source to heat the cold air in severely cold regions in China. The results showed an average temperature rise of 12.4−14.0 ºC provided by EAHE in winter. Studies have shown that EAHEs have the potential to lower the energy consumption in winter and reduce the peak electrical demand in summer.

By coupling SC with EAHE, the cooling and heating performances of SCs can be improved by taking advantage of geothermal energy. The system ventilation operates with solar energy as the driving force and the soil as a heat sink/source. The air is heated in the SC, and buoyancy is generated to extract the indoor air from the building. Consequently, the outdoor air is induced into the interior of the building through EAHE and is pre-cooled/pre-heated by the surrounding soil. Accordingly, the energy

consumption can be further reduced, as the fan is not a necessary component for the EAHE in this coupled SCEAHE system. Among the few studies on coupled SCEAHE systems, Maerefat and Haghighi [30] first proposed the SCEAHE system and attempted to ascertain the system's ability numerically to provide comfortable indoor conditions. It was concluded that achieving indoor thermal comfort is possible by means of proper modifications to the system, even when the environmental conditions are harsh. However, when the outdoor air temperature was too high (approximately 45 °C or more), the SC was no longer suitable. Li et al. [31] investigated the cooling performance of an SCEAHE system during summer. Experimental results showed that the indoor air temperature remained primarily in the range of 21−24 °C, while the outdoor air temperature during the daytime could be as high as 34 °C. The performance of the coupled system largely depended on its cooling capacity. Li et al. [32] experimentally found that under the combined effects of the building thermal mass and SC, 24 h natural ventilation could be achieved for the SCEAHE system in summer. The airflow rate recorded during the day could reach as high as 252 m^3/h. A relatively steady airflow rate of 50−70 m^3/h was achieved because of the building thermal mass when the solar radiation intensity was low or zero.

Although the performance of the SCEAHE system in summer has been studied both numerically and experimentally, the ventilation performance of the coupled system in the transition seasons has not been investigated. Traditionally, SC solo has been used to enhance the natural ventilation along with the opening window (called window-in and SC-out natural ventilation). However, it is unclear whether the conventional ventilation method can create a more comfortable indoor environment during transition seasons, compared to the SCEAHE system. This is important for the SCEAHE system, as the system cost effectiveness can be improved significantly if it is ascertained that the SCEAHE system could operate with an annual cycle. Therefore, an in-depth understanding of the positive contribution by the coupled system in transition seasons is required to complement the natural ventilation performance of the coupled system in different seasons.

This study aims to investigate the natural ventilation performance of the SCEAHE

system experimentally during the transition seasons. The natural ventilation rate, temperature profile, moisture content variation in the air within the EAHE pipe, temperature of the absorber plate in the solar collector, temperature variation of the surrounding soil, and indoor air temperature, were analysed in detail. Meanwhile, the natural ventilation performances of SC solo operation with different window-opening patterns were examined. The results were quantitatively evaluated and have been comparatively analysed, offering quantitative evidence of the SCEAHE compared to the traditional natural ventilation methods. Furthermore, they reinforce the existing literature through experimental results.

2. Experimental setup and procedures

2.1 Experimental test rig

The experimental test rig was located in a region, which is cold in winters, hot in summers, and has relatively mild transition seasons (Tongling City, Anhui Province, China). As shown in Fig. 1(a), the full-scale test rig consists of an EAHE pipe, two chambers, a solar collector, and a vertical chimney. The EAHE pipe outlet and solar collector inlet were only connected to the test chamber, which was used for the investigation of the indoor thermal environment. When solar irradiation was sufficient, the temperature of the air within the solar collector increased owing to the heat transfer from the absorber plate. Then, the reduced air density, in addition to the stack effect of the vertical chimney, generated buoyant pressure that drove the airflow upward. Therefore, ambient air was introduced into the EAHE pipe and was cooled/heated by the surrounding soil, providing cooling/heating capacity and fresh air for the test chamber. During night, in the absence of solar intensity, the heating effect of the subsoil replaces the role of the solar collector, as the nocturnal ambient air temperature is low during the transition seasons. The heating effect of the subsoil, in addition to the height difference between the EAHE inlet and vertical chimney outlet, maintains the buoyancy and airflow rate to some degree. However, it is unclear whether the flowing air heated

by the subsoil can be further heated by the thermal mass, and it needs to be revealed by the experimental results.

The dimensions of the buried pipe, solar collector, and vertical chimney were determined based on the authors' previous numerical simulation work (see Ref. [33]). The PVC EAHE pipe had a diameter of 0.3 m and consisted of an inclined inlet pipe, a horizontal pipe, and a vertical outlet pipe. The 45° inclined inlet pipe was designed to reduce the minor loss at the bend, while the outlet pipe was constructed to be vertical for a more accurate measurement of the radial air velocity profile at the outlet cross section. The 30 m long horizontal pipe was buried 3 m below the ground. The inclined inlet pipe and vertical outlet pipe were both insulated using polystyrene, and the flowing air within the EAHE was primarily cooled/heated by the inner surface of the horizontal pipe. A solar collector with dimensions 7 m (length) × 1.5 m (width) × 0.3 m (height) was installed on the roof to heat the exhaust air. The surface of the absorber plate in the solar collector was coated with a highly absorptive black paint. The tilt angle of the solar collector was chosen as 30° to increase the daily absorbed solar irradiation. The four sides of the solar collector and the back of the absorber plate were insulated to reduce the heat loss using polystyrene boards. The 6 m long vertical chimney with diameter of 0.3 m was connected to the solar collector outlet to enhance the stack effect, and its outer surface was insulated.

A southwest oriented test chamber with dimensions 3 m (length) × 3 m (width) × 3 m (height) was built using perforated brick. The chamber height was chosen to be close to the storey height of a real building, while the floor area was considered as a practical minimum for a real single room. The overall thermal conductivities of the four exterior walls and roof were within the range specified by the "National design standard for building energy efficiency" (GB 50189-2015) [34]. This allows the reproduction of the heat transfer through the building envelop and heat storage in envelop under real conditions. Unwanted wind pressure and rainwater were blocked using two rain hats at the EAHE inlet and vertical chimney outlet, respectively. Fig. 1(b) shows the actual experimental setup.

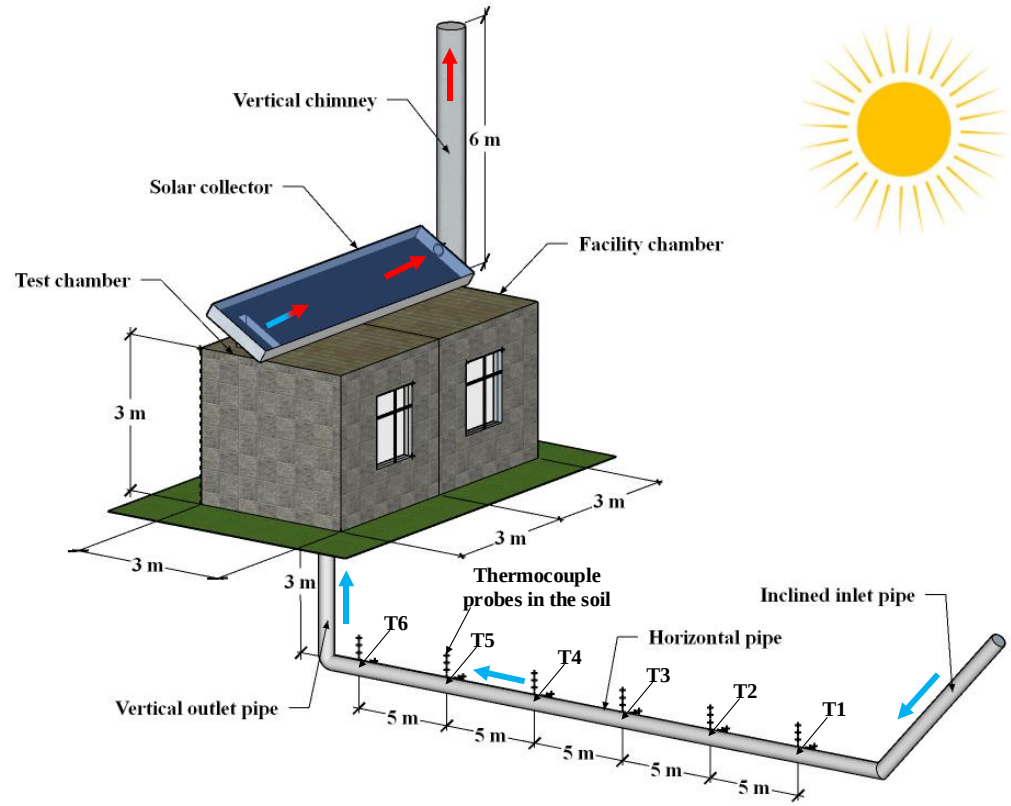

(a) Schematic view

(b) Experimental setup

Fig. 1. Experimental test rig of the SCEAHE system

2.2 Measurement procedure and instrumentation

To evaluate the performance and confirm the advantage of the SCEAHE system in the transition seasons, three operating modes, indicated as A, B, and C, are proposed.

Mode A: The SC operates with the EAHE with the window closed and generates a buoyant driving force for the EAHE when the solar irradiation is strong. Outdoor air is induced into the test chamber only though the EAHE pipe, in which the fresh air is pre-cooled/pre-heated by the surrounding soil. The heating effect of the subsoil replaces the role of the solar collector in inducing the buoyant force and driving the natural airflow when the solar irradiation is weak.

Mode B: The EAHE pipe is closed, and the window is opened. Fresh air is directly induced into the test chamber through a window by the buoyant force generated by the SC or thermal mass. This is a traditional natural ventilation method. It has been called 'window-in and SC-out natural ventilation' in this study. For comparison purposes, the opening area of the window is the same as the cross-sectional area of the EAHE pipe in Mode A.

Mode C: This mode is designed to investigate the effect of window opening area on the ventilation performance. In this mode, the operating mechanism is the same as that in Mode B, while the opening area of the window is twice that in Mode A.

Schematics of the three operating modes are shown in Fig. 2. For comparative purposes, the experimental test lasted for 6 d under similar weather conditions, and each mode operated for 2 d to ensure the reliability of the experimental results. The test dates and corresponding operating conditions are listed in Table 1.

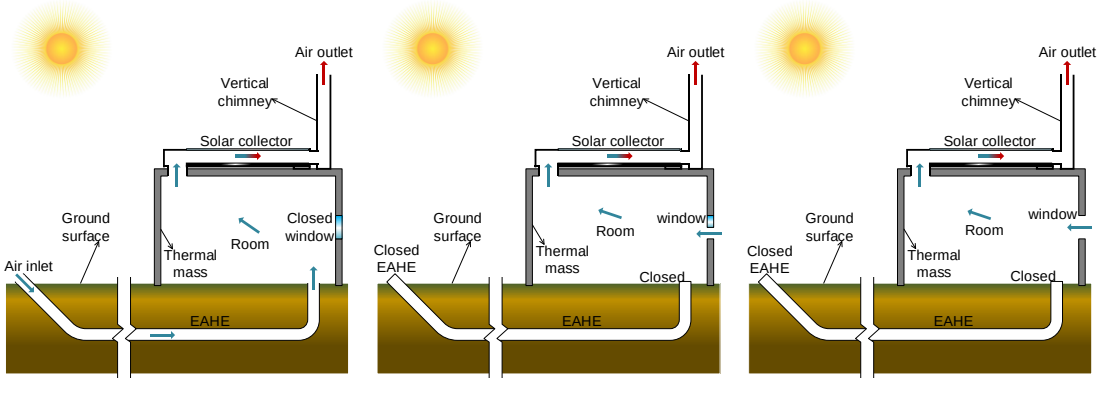

Fig. 2. Three experimental operating modes

Table 1. Test dates and corresponding operating conditions

Date	Oct. 29−Oct. 30	Oct. 31−Nov. 01	Nov. 02−Nov. 03
Duration	48 h	48 h	48 h
Mode	A	B	C
EAHE	Open	Closed	Closed
Window	Closed	Open	Open
Ventilation area (m^2)	0.071	0.071	0.142

To measure the air temperature variation along the flow path, as shown in Fig. 1(a), six thermocouples (T1–T6) were equidistantly spread along the centre line of the EAHE horizontal pipe, with 5 m distance between the adjacent measuring points. In addition, at each temperature measuring point in the horizontal pipe, to measure the temperature fluctuations in the surrounding soil, three thermocouple probes were placed in the soil at distances of 0.15 m, 0.3 m, and 0.45 m from the pipe surface along both the vertical and horizontal radial directions (Fig. 3(a)). As shown in Fig. 3(b), three thermocouples were evenly spread in the centre line of all the outer and inner surfaces of the four exterior walls and roof of the test chamber to obtain the temperatures of the envelope enclosure. The radiant heat transfer, which may cause error, was blocked using aluminium films. The indoor air temperatures were measured using three thermocouples at distances of 1.1 m, 1.7 m, and 3 m from the floor of the test chamber. To measure the temperature profile of the flowing air for the solar collector channel, eight thermocouples (SC-A1–SC-A8) were evenly spread in the centre plane (Fig. 3(c)), which is equidistant from both the glass cover and absorber plate (0.15 m away from the absorber plate), along the length and width directions. Four thermocouples were equidistantly spread along the centre line of both the glass cover and absorber plate surface to obtain their temperatures (SC-G1–SC-G4 and SC-S1–SC-S4). The air temperatures at the solar collector inlet and outlet were measured using three

thermocouples placed along the inlet and outlet centrelines. All the probes used for the solar collector were shielded using aluminium films. For the exterior walls and roof of the test chamber, inlet and outlet cross section of the solar collector, and the absorber plate and glass cover, the values of the multiple temperature measuring points on them were averaged to represent their temperatures. All the thermocouple probes were calibrated before use. The air velocities at the EAHE outlet were obtained using three air velocity sensors (Omega FMA902A-MA), and their positions were chosen according to the ring method of the equivalent area [35, 36], as shown in Fig. 3(d). The measured temperature and air velocity data were transmitted to a data acquisition instrument (Agilent 34980A) and a transmission module, respectively, every 60 s, and were finally collected and saved on a computer. The temperature and relative humidity of the air at the EAHE inlet and outlet were recorded using two temperature and humidity meters (HIOKI 3641-20). A solar power meter (TBQ-2) was used to measure the solar intensity.

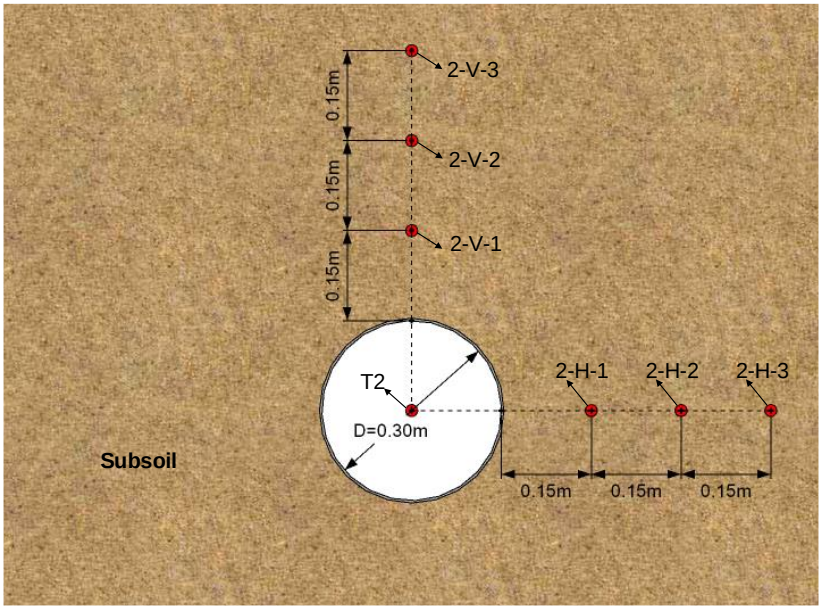

(a) Locations of thermocouples in the subsoil along the vertical and horizontal directions (10 m from the horizontal pipe inlet)

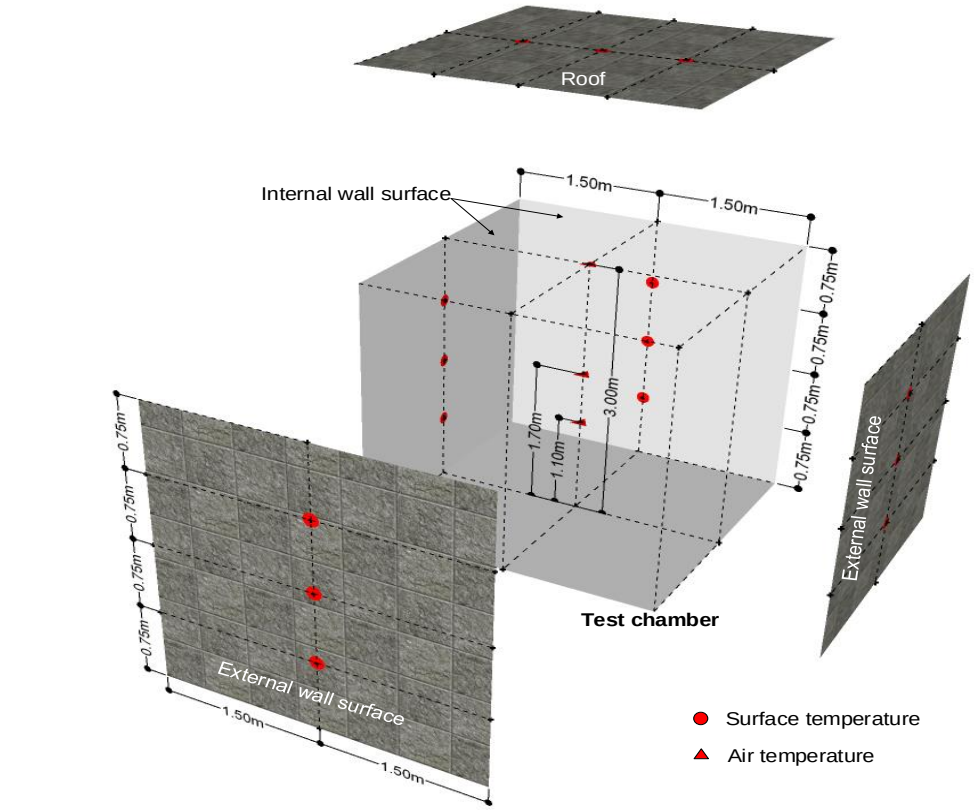

(b) Locations of thermocouples on the test chamber surfaces and inside the test chamber

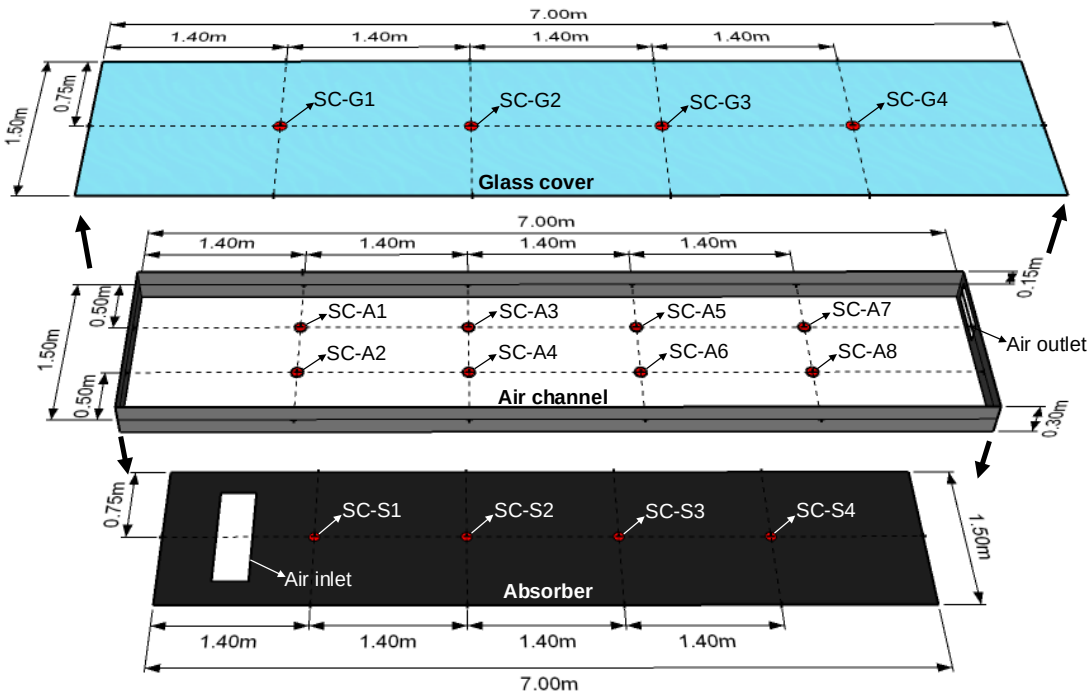

(c) Locations of thermocouples on the absorber, glass cover, and inside the air channel

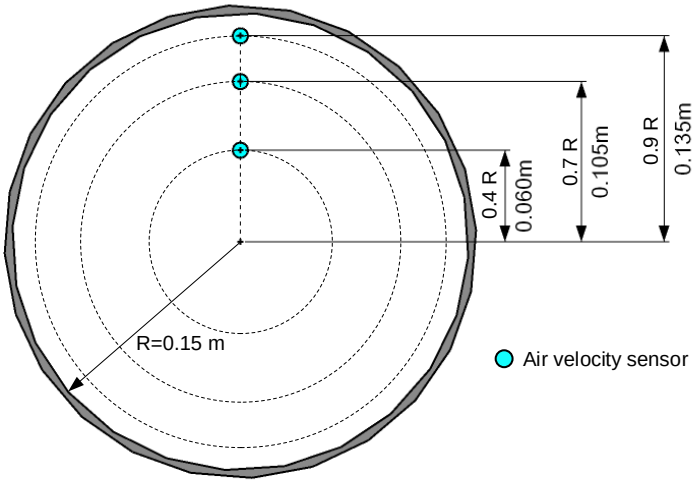

(d) Locations of air velocity sensors at the EAHE outlet

Fig. 3. Distributions of measuring devices

2.3 Uncertainty analysis

The random uncertainty and system uncertainty were calculated using Eqs. (1) and (2), respectively, based on statistical analysis and uniform distribution [37].

$$\sigma_i = \sqrt{\frac{\sum_{i=1}^{n}(x_i-\bar{x})^2}{n-1}}, \quad (1)$$

where σ_i is random uncertainty, x_i is a single measurement value, $\bar{x}$ is the averaged measurement value, n is the number of measurements.

$$\mu_i = \frac{e_i}{\sqrt{3}}, \quad (2)$$

where μ_i is system uncertainty; e_i is instrumental error.

The random and system uncertainties were merged using Eq. (3) [37].

$$\sigma = \sqrt{\sum_{i=1}^{m_1}{\sigma_i}^2 + \sum_{i=1}^{m_2}{\mu_i}^2}, \quad (3)$$

where σ is the merged uncertainty, m_1 is the number of random uncertainties, m_2 is the number of system uncertainties.

The details of the instruments and calculated maximum error margin with a confidence

interval of 99 % using Eqs. (1)–(3), are presented in Table 2.

Table 2. Specifications and error margins of different measurement devices.

Device	Type	Measuring range	Accuracy	Maximum error
K-type Thermocouples	Omega SA3-K-120	−17 °C to 260 °C	±0.5 °C	2.29%
K-type threaded probe thermocouples	WRNT-01	0 °C to 800 °C	±0.5 °C	2.65%
Humidity and temperature meter	HIOKI 3641-20	Temperature: −20.0 °C to 70.0 °C	Temperature: ±0.5 °C	2.77%
		Relative humidity: 0.0% to 100.0%	Relative humidity: ±5%	6.86%
Airflow sensors	Omega FMA902A-MA	0 m/s to 5.08 m/s	±2%	2.67%
Solar radiation meter	TBQ-2	0–2000 W/m^2 280–3000 nm	< 2%	2.36%

2.4 Experimental calculations

The air flow rate V (m^3/h) at the EAHE outlet was obtained using Eq. (4).

$$V = 3600\pi R^2 v, \tag{4}$$

where R is the pipe radius (m), v is the average air velocity at the EAHE outlet (m/s). The cooling or heating power Q (W) was calculated using Eq. (5).

$$Q = \frac{c\rho V(T_{in}-T_{out})}{3600}, \tag{5}$$

where T_{out} and T_{in} are the air temperatures at the EAHE outlet and inlet, respectively (°C); c is the specific heat of air, J/(kg· °C); ρ is the air density (kg/m^3); V is the air flow rate (m^3/h).

The moisture content ω (kg/kg) at the EAHE inlet and outlet was obtained using Eq. (6) [35].

$$\omega = 0.622\varphi \frac{P_s}{(P_0-\varphi P_s)}, \tag{6}$$

where φ is the relative humidity of air (%), P_s is the saturated vapour pressure (Pa), P_0 is the local atmospheric pressure (Pa).

A computationally effective formulation was suggested by Pátek and Klomfar [38] to calculate P_s:

$$P_s = P_c \times \exp\left[\frac{T_c}{T}\sum_{j=1}^{6}\alpha_j\left(1-\frac{T}{T_c}\right)^{\beta_j}\right], \quad (7)$$

where T is water temperature (K). The calculation coefficients $\alpha_1-\alpha_6$, $\beta_1-\beta_6$,P_c, and T_c are listed in Table 3 [38].

Table 3. Calculation coefficients for Eq. (7).

j	β_j	α_j
1	1.0	-7.85951783
2	1.5	1.84408259
3	3.0	-11.7866497
4	3.5	22.6807411
5	4.0	-15.9618719
6	7.5	1.80122502

T_c=647.096 K; P_c=22.064×10^6 Pa

3. Experimental results and discussions

3.1 Solar irradiation and outdoor air temperature

The measured outdoor air temperatures and solar irradiation during the testing period are depicted in Fig. 4. As shown, the weather from October 29 to November 3 was fair, and the daily outdoor air temperature and solar irradiation were patterned similarly and periodically. The daily solar intensities varied in the range 0−820 W/m^2, and the outdoor air temperature was in the approximate range of 12.5−25.0 °C with a diurnal temperature fluctuation of 12.5 °C. It was observed that daytime natural ventilation is appropriate for buildings, as the air temperature of the external environment falls within the comfort limits [39]. In contrast, the nocturnal outdoor air temperature may not be preferable for natural ventilation because the air temperature is low and would cause discomfort.

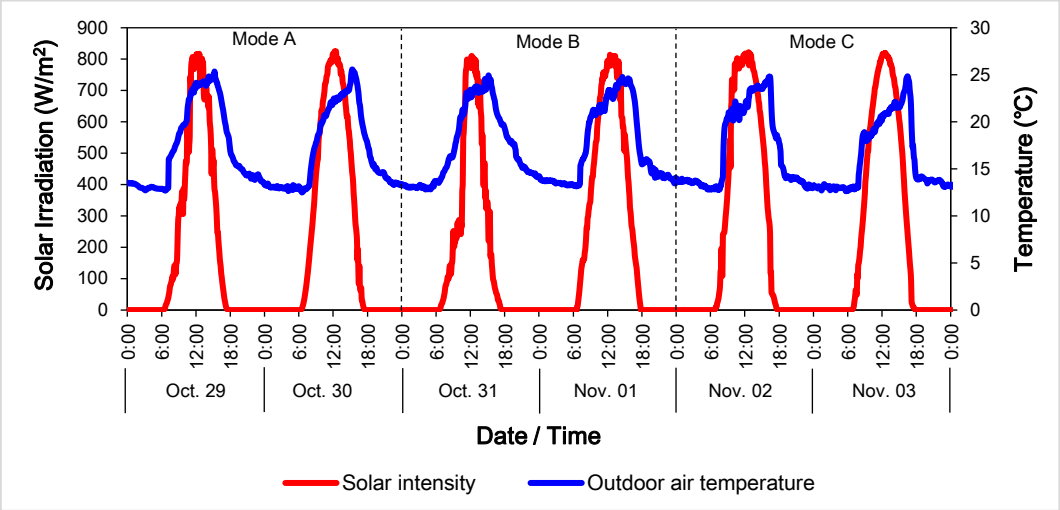

Fig. 4. Outdoor air temperature and solar irradiation during testing period

3.2 Comparison of different operating modes

3.2.1 Airflow rates for the three modes

The measured airflow rates for Modes A, B, and C are plotted in Fig. 5. It can be observed that the continuously and periodically fluctuating airflow rate was induced by the SCEAHE system over the testing period. The variation in airflow rate is closely related to the solar intensity variation during the daytime. This is because the solar radiation heats the solar collector surface and draws the SC draft power, consequently increasing the airflow rate. Although the solar irradiation was insufficient from 17:00 to 06:30, the airflow rate was still recorded. It has been further discussed in Section 3.2.3**.** Therefore, the feasibility of 24 h continuous natural ventilation was verified for each operating mode.

Specifically, the patterns of the airflow rate were approximately the same in each mode. For Mode A, the airflow rate gently varied in the range 130−150 m^3/h between 00:00 and 08:00, despite the recorded solar radiation between 05:00 and 08:00. After 08:00, the airflow rate swiftly increased until 12:30 and reached a maximum value of 255 m^3/h. After 16:00, the airflow rate swiftly declined to approximately 110 m^3/h at 17:30, and then slowly increased afterwards. In Mode A, the average daytime and nocturnal airflow rates for two continuous testing days were 209 m^3/h was 139 m^3/h, respectively.

A distinct sharp drop exists in the airflow rate at 0:00 October 31 when the operating mode changed from Mode A to Mode B. This is because the outdoor air is directly drawn into the indoor space through the open window rather than through the EAHE pipe in Mode B. The induced low-temperature ambient air narrowed the temperature difference between the indoor and outdoor air and reduced the buoyant pressure. The airflow rate fluctuated around 110 m^3/h until 08:00, and then sharply increased to a maximum value of approximately 388 m^3/h. The airflow rate dropped rapidly to approximately 90 m^3/h after 17:30 h. In Mode B, the average daytime and nocturnal airflow rates for two continuous testing days were 286 m^3/h and 87 m^3/h, respectively. In Mode C, the maximum and average daytime airflow rates were 410 m^3/h and 340 m^3/h, respectively, while the average nocturnal airflow rate was 80 m^3/h.

Furthermore, the average daytime airflow rate for Mode C was 18.9 % higher than that for Mode B and 62.7 % higher than that for Mode A. The average nocturnal airflow rate for Mode C was 8.0 % lower than that for Mode B and 42.4 % lower than that for Mode A. This is because the buoyant driving force is sensitive to the pressure drop caused by various system components. Although the outlet area of the EAHE pipe in Mode A was the same as that of the open window in Mode B, the pressure drop induced in the EAHE pipe was much larger than that induced by the window. The pressure drop further decreased when the opening area of the window doubled in Mode C. The high daytime ventilation, in addition to the nocturnal ventilation with low temperature eliminated more heat stored in the thermal mass, and in turn reduced the temperature difference between the inside and outside of the building.

It should be noted that although the opening area was increased by 100 % in Mode C, the airflow rate was increased by only 18.9 % compared to that in Mode B. This can be attributed to the relatively low resistance ratio of the window opening compared with that of the solar chimney. Hence, the airflow rate was less sensitive to the window opening area when it doubled, and the effect of the ventilation area on this system was not as significant as expected.

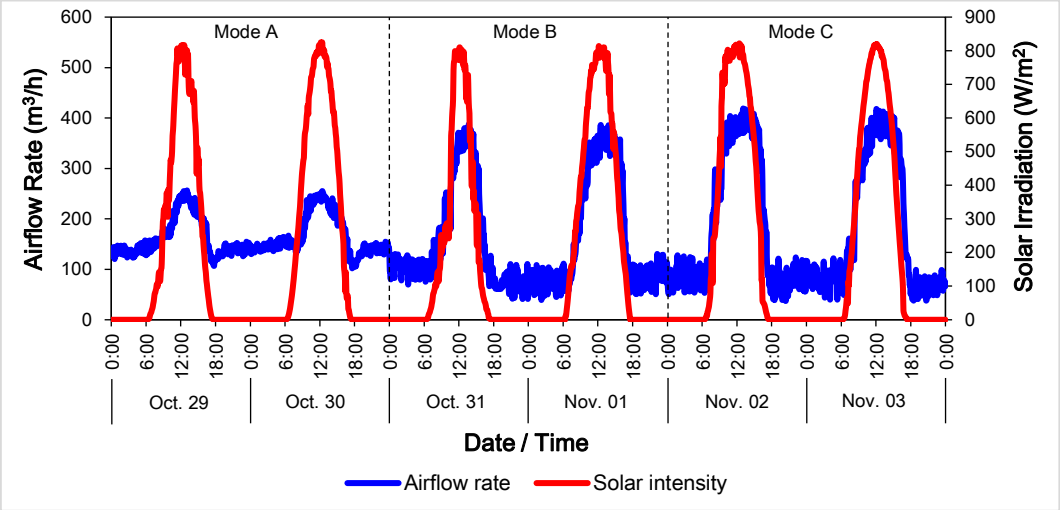

Fig. 5. Airflow rate and solar irradiation during the testing period

3.2.2 Comparison of the temperature profiles of the heated absorber

For an SC, the generated buoyancy depends primarily on the surface temperature of the absorber. Fig. 6 shows the variations in the average surface temperature of the absorber for the three operating modes. It can be seen that the surface temperature values of the absorber were approximately the same and varied slightly around 15 °C before 07:00. From 08:00 onwards, the temperature of the absorber plate rose dramatically, and the surface temperature for Mode A started to exceed that for Mode B, which exceeded that for Mode C. This phenomenon can be attributed to the higher airflow rates drawn in Modes B and C. The higher airflow rate enhanced the heat transfer between the flowing air and collector surface, leading to a higher reduction in the surface temperature compared to that in Mode A. The peak surface temperature for Mode A was approximately 75 °C, while that for Modes B and C was approximately 71 °C and 69 °C, respectively. The high surface temperature created sufficient draft power during the daytime. The surface temperatures dropped sharply after 14:30, and the difference between them vanished as soon as they were approximately 15 °C at 18:00. Then, the temperature varied slowly. The obtained results indicated that a higher airflow rate resulted in a lower absorber plate temperature and corresponded to a lower buoyant force. This is another reason for the ventilation rate being not as high as that expected in Mode C.

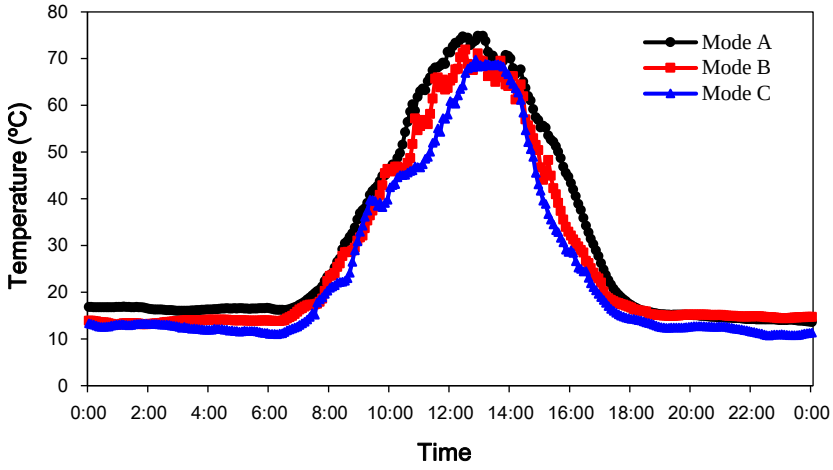

Fig. 6. Average absorber surface temperatures for the three operating modes

3.2.3 Nocturnal ventilation driving force

For stack-driven natural ventilation, one of the most important factors affecting the ventilation rate is the difference between the indoor and outdoor air temperatures, as it is proportional to the generated buoyant force.

Fig. 7 shows the indoor and outdoor air temperatures during the testing period. In Mode A, between 9:30 and 16:30, the indoor air temperature was lower than the outdoor air temperature, and the maximum temperature difference reached 2.5 °C. At this stage, the draft power generated by the SC played a major role in chamber ventilation. The temperature difference between the indoor and outdoor air decreased as the outdoor air temperature gradually decreased. During the periods of 00:00 to 09:30 and 16:30 to 23:59, the average temperature of the indoor air was 5.2 °C higher than that of the outdoor air, and the airflow rate was in the range 110−150 m^3/h. At these two stages, the heating effect of the subsoil played a major role in generating buoyancy, as solar irradiation was absent.

For Modes B and C, although the temperature difference between indoor and outdoor air could be ignored during daytime, as the ambient was directly induced inside the chamber, there were air temperature differences with average values of 3.6 °C and 3.0 °C, respectively, during the night. Therefore, the nocturnal airflow rates in Modes B and C were lower than those in Mode A. Ref. [32] reported that a relatively steady airflow rate of 50−70 m^3/h was maintained by the thermal mass during the night as

there was no considerable difference in the indoor and outdoor air temperatures in the summer season. However, the temperature difference increased further in the transition seasons, which resulted in a higher night ventilation rate. Furthermore, although nocturnal ventilation was created in all the three modes, the source of the driving force in Mode A was not the same as that in Modes B and C.

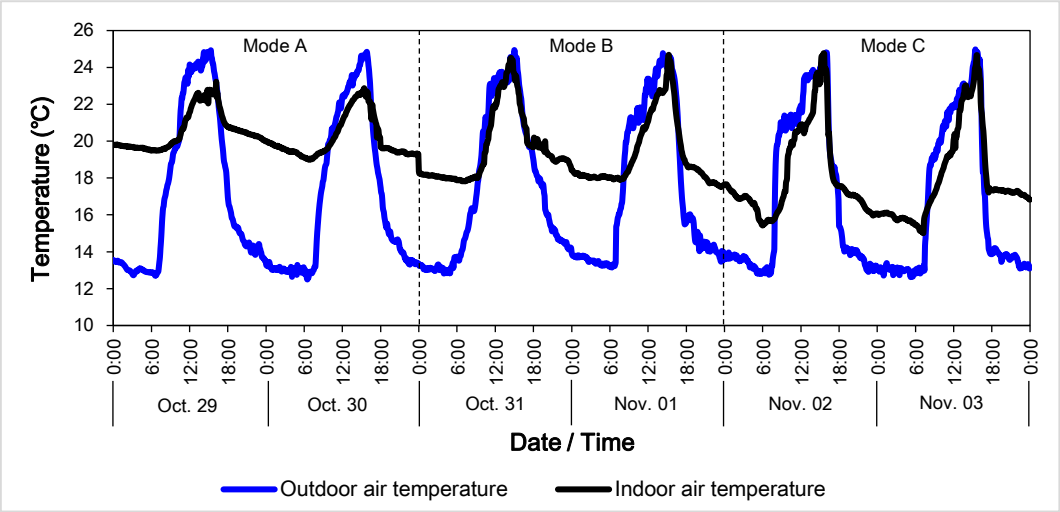

Fig. 7. Indoor and ambient air temperatures during the testing period

3.2.4 Variations in EAHE inlet and outlet air temperature and relative humidity

Fig. 8 depicts the average temperatures of the EAHE inlet and outlet air on October 29 and 30. It is evident that the temperature variation at the EAHE outlet was weakened significantly by the EAHE. The outlet air temperature from the EAHE rarely changes over 24 h. When the inlet temperature changed from 12.5 °C to 25.0 °C, the outlet temperature varied from 21.4 °C to 23.0 °C, and the fluctuation range was only 1.6 °C. In addition, the air temperature difference exhibited a trend similar to that of the ambient air temperature; however, it was not always positive. This indicated that the outdoor air was heated and cooled in Mode A. The EAHE operated under the heating conditions when the soil was warmer than the ambient air. Airflow through the EAHE pipe allowed for the extraction of heat from the surrounding soil. EAHE effectively elevated the fresh air temperature with a maximum increase of 8.0 °C. However, as soon as the ambient air temperature rose above that of the soil during daytime, excess

heat was stored in the soil again. Thus, the EAHE operates under cooling conditions. The fresh air temperature was reduced by as much as 2.5 °C. The heating and cooling capacities of the SCEAHE system were beneficial to indoor thermal comfort.

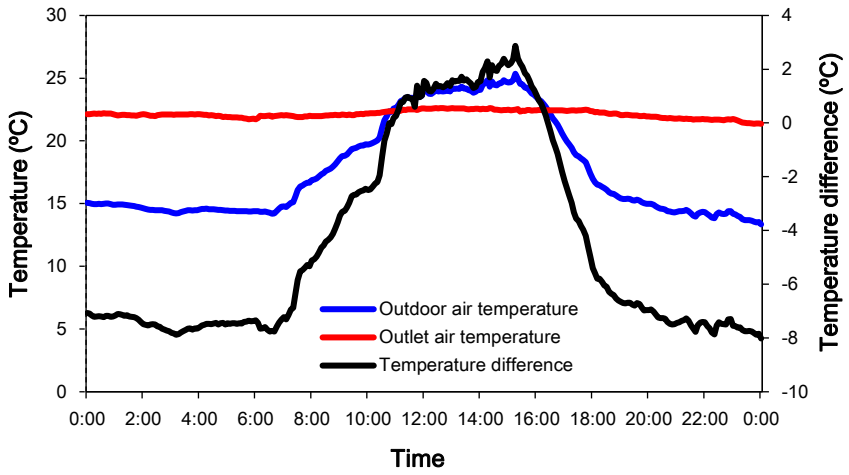

Fig. 8. Average temperatures of EAHE inlet and outlet air on October 29 and 30

As shown in Fig. 9, it is evident that there is a significant difference between the relative humidity at the inlet and outlet of the EAHE, while the moisture content at the inlet and outlet showed slight differences, indicating that neither humidification nor condensation occurred during the heat transfer process inside the EAHE in Mode A. It is known that moisture content is closely related to the air temperature and relative humidity. Referring to the inlet and outlet air temperature data in Fig. 8, although the relative humidity at the inlet was comparatively high, the moisture content was maintained at a low level because of the low ambient temperature during the night. Thus, the outlet relative humidity decreased as the outlet air temperature increased after the heating process. In contrast, the relative humidity at the inlet was relatively low during the daytime because of the comparatively high ambient air temperature, and the outlet relative humidity increased as the outlet air temperature decreased after the cooling process.

Similar to the outlet air temperature, the variation in the outlet relative humidity was attenuated by EAHE significantly. The inlet relative humidity changed from 43.8 % to 98.1 %, while the outlet relative humidity varied only between 61.9 % and 79.2 %.

Furthermore, the nearly constant air moisture content indicated that only sensible heat transfer occurred during the transition seasons.

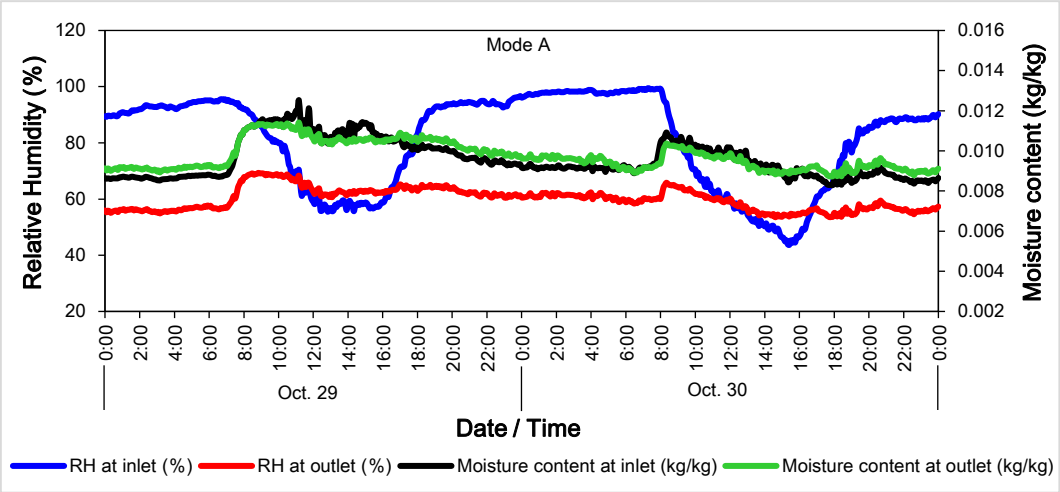

Fig. 9. Relative humidity and moisture content of the EAHE inlet and outlet air in Mode A

3.2.5 Heating and cooling power

Heating or cooling capacity is one of the critical factors for evaluating the performance of the SCEAHE system, although the prior consideration is to provide fresh air for buildings in the transition seasons. According to the temperature and moisture analysis, sensible heat transfer occurred primarily inside the EAHE during the transition seasons. Thus, the heating or cooling power was calculated using Eqs. (4) and (5), and are presented in Fig. 10.

As shown in Fig. 10, a relatively steady heating power (varied around 350 W) was recorded from 21:00 to 7:30. Between 7:30 and 11:00, owing to the rise in the ambient air temperature and decrease in the temperature difference for EAHE heat transfer, the heating power gradually decreased to zero. Then, from 11:00 on, as the ambient air temperature rose above that of the soil during daytime, excess heat was stored in the soil; thus, the EAHE provided cooling power for the test room. The maximum cooling power reached 200 W at 15:00, matched with the highest outdoor air temperature of approximately 25 °C. As the outdoor air temperature gradually decreased from 15:00, the EAHE pipe shifted from providing cooling capacity to providing heating capacity

at 16:30, and the heating power reached approximately 350 W at 21:00. It is evident that the heating or cooling power is highly associated with the inlet air temperature of the EAHE, as the temperature of the soil surrounding the pipe is relatively steady. The overall heating and cooling capacities for 24 h were calculated to be 19474 kJ and 2179 kJ, respectively. Their ratio was approximately 9:1. Therefore, extracting heat from the soil dominated the heat transfer process between the fresh air and surrounding soil, which caused a decrease in the soil temperature.

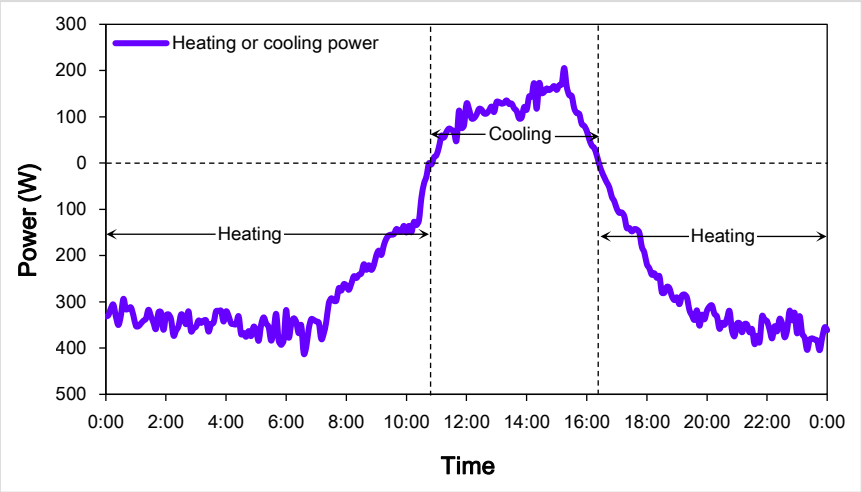

Fig. 10. Average heating or cooling power in Mode A

3.2.6 Temperature variations of soil

Fig. 11 illustrates the variations in the subsoil temperature of the vertical and horizontal measuring points at a distance of 0.15 m from the EAHE pipe. At the beginning of the test period, the soil temperatures along the pipe length were not identical regardless of whether it was in the vertical direction or in the horizontal direction but varied within in the range of 23.5−24.0 °C. Furthermore, the soil temperature variations at different locations had a similar trend and showed a strong correlation with the ambient air temperature over the test period. Although the EAHE was operated to pre-heat/pre-cool the ambient air, the overall variation in the soil temperature decreased in Mode A. It is evident that the soil temperature had a distinct drop near the inlet part of the EAHE, as the temperature difference for heat transfer was largest at this part of the EAHE. However, the soil temperature variation became gentler along the pipe length, as the

temperature difference between the flowing air and soil was reduced along the flow path. Between 00:00 and 07:00, all soil temperatures decreased as the outdoor air temperature was low during this period. Thus, the subsoil surrounding the buried EAHE pipe was continuously cooled by ambient air. After 07:00, the thermocouples along the vertical and horizontal directions recorded a decrease in temperature, although the outdoor air temperature increased. This is because the large thermal inertia of the soil delayed the thermal response of the soil. The subsoil temperature approached the minimum at approximately 12:00. Then, the ambient air temperature dropped sharply from 15:00, while the soil temperatures increased until 19:00, and then decreased again until 24:00. The subsoil temperature variation trend followed a similar pattern in the next day (October 30). After the two-day continuous operation (from October 29 to October 30), the soil temperatures at a distance of 5 m from the inlet of the horizontal pipe along the vertical (1-V-1) and horizontal directions (1-H-1) dropped by 0.78 °C and 0.74 °C, respectively. The decreased temperatures 30 m away from the entrance of the EAHE were only 0.46 °C and 0.44 °C, respectively.

In Modes B and C (from October 31 to November 3), the EAHE pipe was closed, and fresh air was directly induced into the test chamber through a window by the buoyant force, while the subsoil was in the recovery period. The soil temperatures in the vertical and horizontal directions still showed a periodic variation, although there was no air flowing through the EAHE pipe during the recovery period, which indicated a substantial influence of climate on the soil temperature at a depth of 3 m. After the four-day recovery period, the soil temperature gradually increased and eventually reached a steady state. Temperature stratification was observed along the pipe length at the end of the recovery period. In other words, the soil temperatures at locations farther from the EAHE inlet were closer to the temperature of the undisturbed soil than that closer to the EAHE inlet. For example, the soil temperatures at locations 6-H-1 and 6-V-1 (30 m away from the EAHE entrance) were 23.73 °C and 23.6 °C, respectively. However, the soil temperatures at locations of 1-V-1 and 1-H-1 (5 m away from the EAHE entrance) were 23.08 °C and 23.03 °C, respectively, which were still lower than that in the initial state because of the influence of EAHE and outdoor climate.

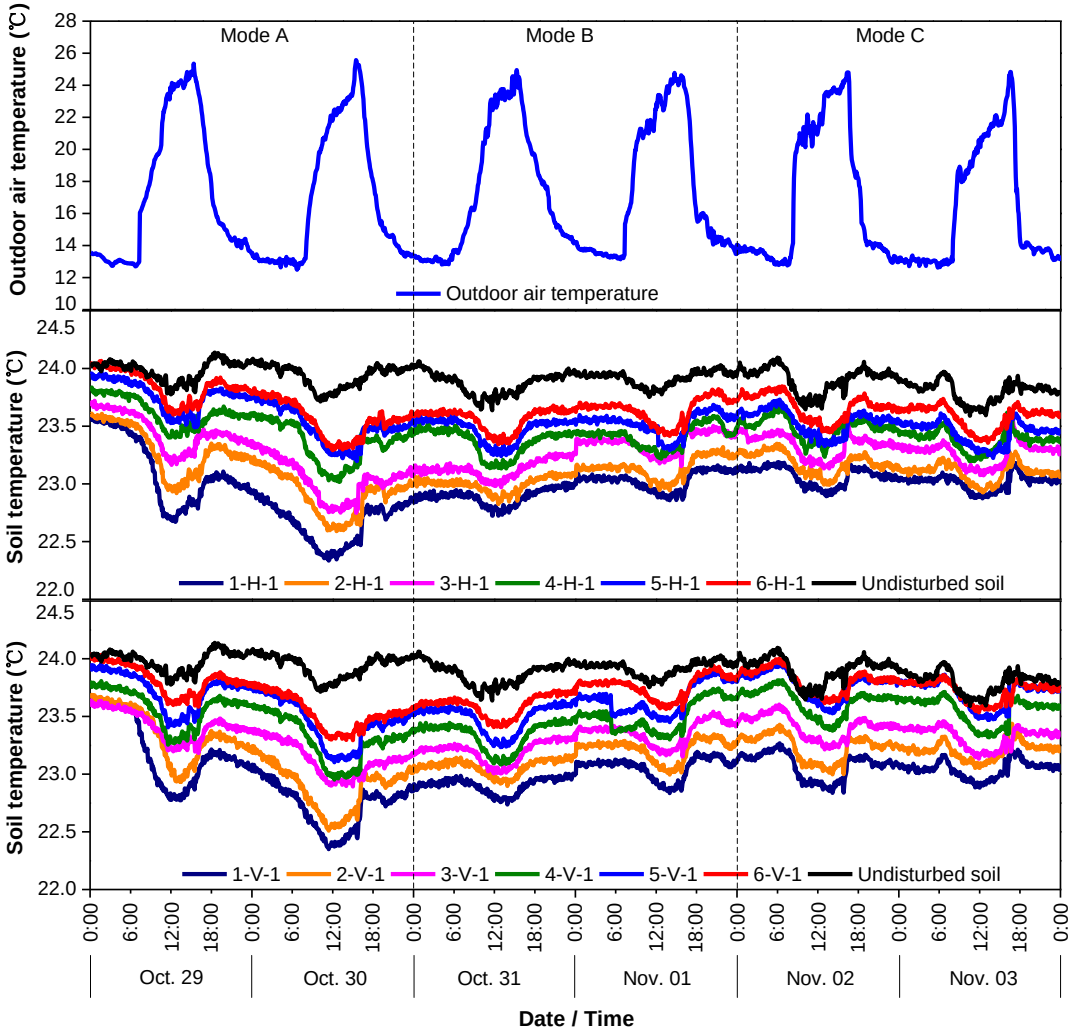

Fig. 11. Variations in the subsoil temperature of the vertical and horizontal measuring points 0.15 m away from the EAHE pipe

Fig. 12 illustrated the variations in soil temperature at distances of 0.15 m, 0.3 m, and 0.45 m from the pipe surface along both the vertical (1-V-1 to 1-V-3) and horizontal (1-H-1 to 1-H-3) radial directions, 5 m away from the horizontal pipe inlet. Additionally, the temperature profiles exhibited a similar variation trend and had a strong relationship with the outdoor air temperature over the test period. The soil temperatures varied with the distance from the EAHE pipe surface, and the temperature change in the soil closer to the pipe surface was more severe than that farther from the pipe in Mode A. When the soil temperatures at distance of 0.15 m along the vertical direction (1-V-1) and horizontal direction (1-H-1) changed by 0.78 °C and 0.74 °C, from October 29 to October 30, respectively, the soil temperatures at a distance of 0.3 m from EAHE pipe

(1-V-2 and 1-H-2) decreased by only 0.35 °C. At the distance 0.45 m away (1-V-3 and 1-H-3) the temperature had an even smaller change of 0.2 °C. As the distance increased, the temperature change decreased, which means that the effect of air on the soil temperature was diminished. Thus, farther the distance, lesser is the influence of air on the soil. Nevertheless, when the operating mode was changed from Mode A to Modes B and C, the soil temperatures at farther distances (0.3 and 0.45 m) first decreased slowly, and then reached a steady state at the end of the test period. The temperature of the soil at a distance of 0.15 m started to increase gradually, and then reached a steady state. This is because the heat absorbed by the soil closer to the EAHE pipe was continuously transferred to the soil farther away from the pipe. The final state of soil temperatures was distinctly lower than that of the initial state because of the strong influence of the EAHE.

According to the analysis, it was concluded that although the soil temperatures 0.15 m away from the pipe surface decreased by approximately 0.74 °C and 0.78 °C in the horizontal and vertical directions, respectively, after the tow-day test, the heating ability of the soil surrounding the EAHE pipe was still strong, as the soil temperatures farther away from the pipe entrance were less affected by the fresh air. In addition, EAHE has the ability to cool and heat the fresh air in transition seasons because of the large diurnal temperature fluctuation, which can help the soil temperature to recover and be beneficial for the application of the SCEAHE system in transition seasons.

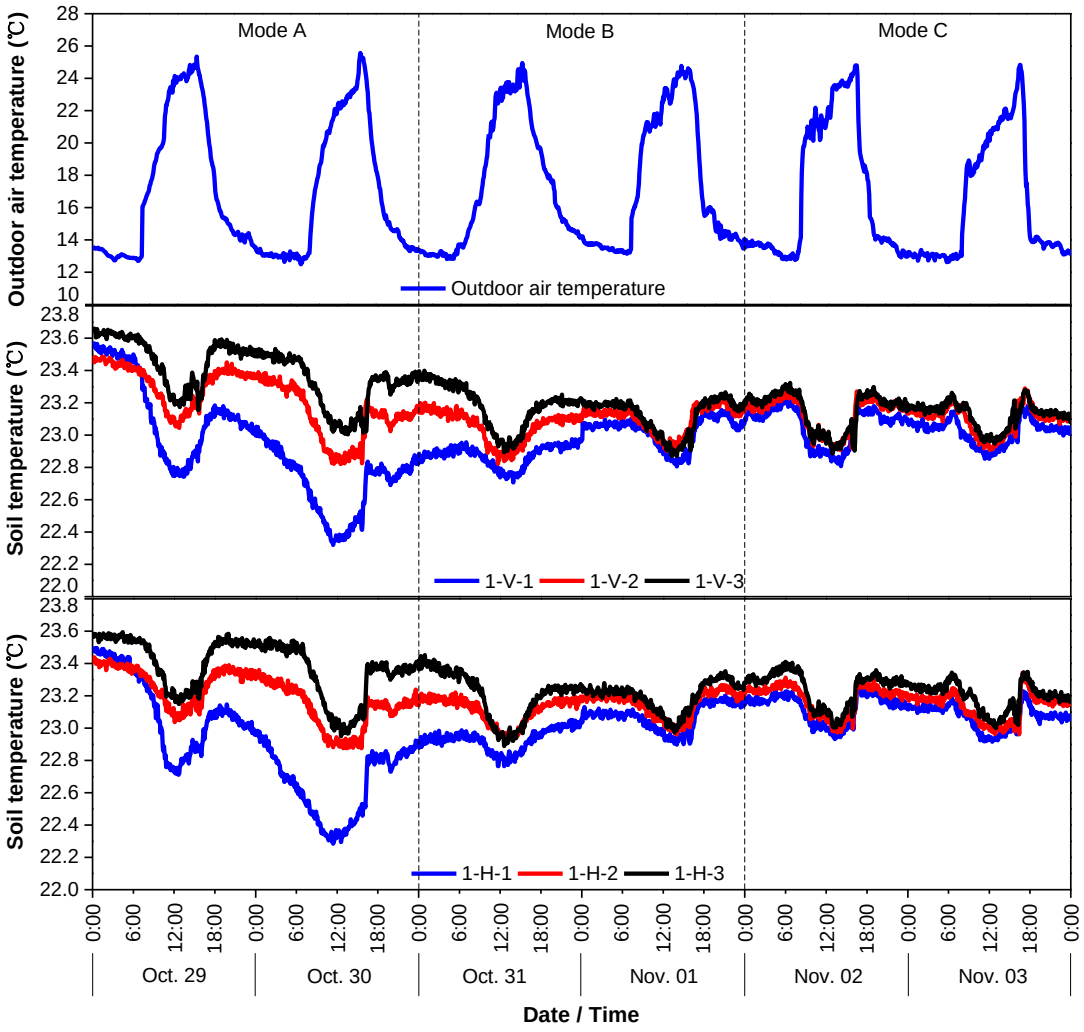

Fig. 12. Variations in the soil temperature 5 m away from the entrance of the horizontal pipe

3.3 Indoor thermal environment

3.3.1 External and internal wall temperatures

The external and internal wall surface temperatures reflect the heat transfer rate between the outdoor and indoor environments. Figs. 13(a)–(b) show the average temperatures of the external and internal wall surfaces of the test chamber for different operating modes. The corresponding external wall surface temperature curves varied in a similar pattern for all the operating modes. The temperature of the external wall of the test chamber for Mode A was used as a sample. As shown in Fig. 13(a), the temperatures at the external surfaces in the east, south, west, and north directions, and

the roof varied in the ranges 11.3–38.6 °C, 11.0–54.6 °C, 11.2–32.8 °C, 11.0–27.5 °C, and 7.7–36.3 °C, respectively. The external wall temperatures varied and differed from each other. The external surface temperature is proportional to the solar radiation intensity absorbed by the corresponding external wall [39]. Furthermore, all the external surface temperatures remained stable during the night, and the temperature of the roof was slightly lower than that of the other walls. This was owing to the nocturnal radiation exchange between the external wall and night sky, and the roof had the strongest nocturnal radiation effect.

As shown in Fig. 13(b), the general variation trends of the internal wall surface temperatures for different operating modes were similar, while the fluctuation amplitudes were different. For Mode A, as shown in Fig. 13(b), the temperatures at the internal surfaces in the east, south, west, north directions, and the roof varied in the ranges 19.4–20.5 °C, 18.8–22.3 °C, 18.8–20.5 °C, 18.3–20.1 °C, and 18.7–21.6 °C, respectively. For Mode B, the internal surface temperatures in the east, south, west, and north directions, and the roof varied within the ranges 18.6–20.3 °C, 17.9–20.9 °C, 18.1–19.6 °C, 17.8–19.4 °C, and 18.0–20.7 °C, respectively. All the internal surface temperatures in Mode B were lower than those in Mode A, as the cool fresh air through the window extracted more heat from the internal walls. For Mode C, the internal surface temperatures in the east, south, west, and north directions, and the roof changed within the ranges 16.9–19.1 °C, 16.0–20.3 °C, 15.8–18.3 °C, 15.7–17.9 °C, and 15.9–19.7 °C, respectively. The internal surface temperatures were reduced further compared to those in Mode B. Furthermore, by comparing the internal and external wall temperatures, it was found that the temperature fluctuation amplitudes of the internal walls were significantly dampened, and the time shift between the internal and external wall temperatures existed because of the thermal storage capacity of the building thermal mass. The external wall temperatures were significantly higher than the corresponding internal wall temperatures during the daytime; however, they were lower than the internal wall temperatures during the night. The existence of a thermal mass can help regulate the indoor environment in transition seasons.

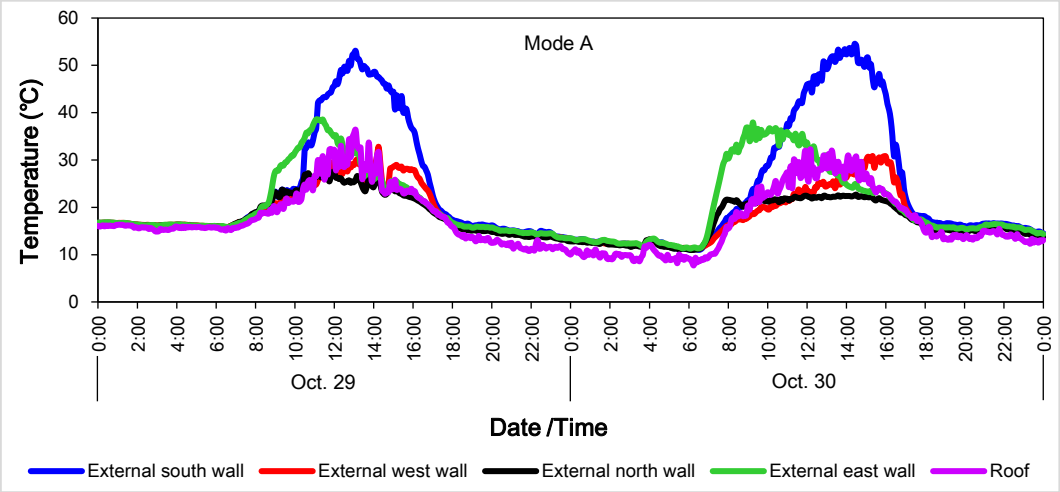

(a) External wall temperature

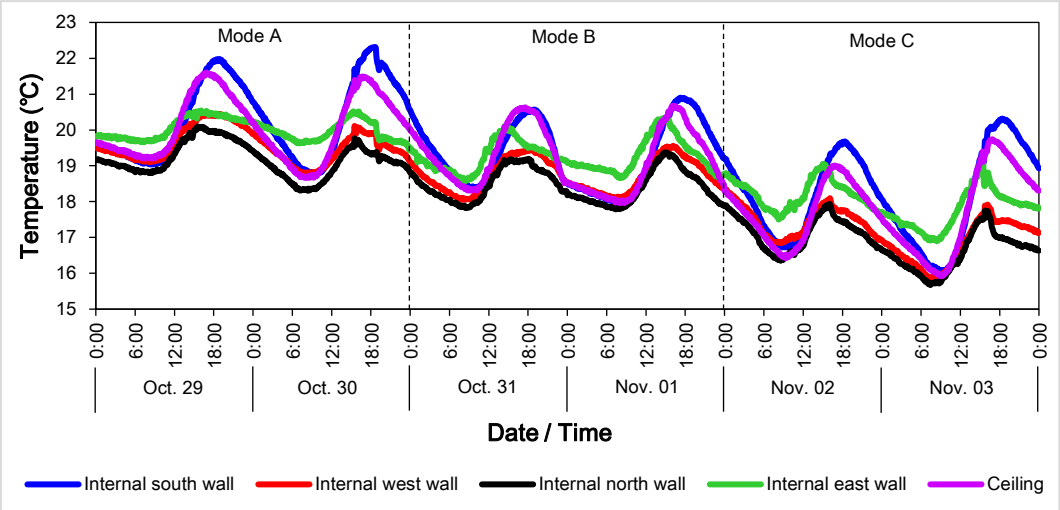

(b) Internal wall temperature

Fig. 13. Average temperatures of the external wall surfaces and internal wall surfaces for different operating modes

3.3.2 Indoor air temperature

The primary task of the SCEAHE system is to provide fresh air and create a comfortable indoor environment; thus, the degree to which the ventilation affects the indoor thermal environment is evaluated. Fig. 14 shows the variations in the average internal wall temperature, indoor air temperature, and outdoor air temperature for the three operating modes. Compared to the outdoor air temperature, the temperature variations in the indoor air and internal wall were considerably attenuated in Mode A. When the outdoor temperature changed from 12.5 °C to 25.0 °C (temperature difference of 12.5 °C),

indoor temperature only varied within a narrow range of 19.7− 22.7 °C (temperature difference of 3.0 °C), and the internal wall temperature fluctuated from 18.9 °C to 20.9 °C (temperature difference of 2.0 °C) during the two-day period. Although the average temperature of the indoor air was 1.8 °C lower than that of the outdoor air from 10:20 to 16:20, it was significantly elevated by 5.1 °C in the remaining time. It was even slightly higher than the internal wall temperature owing to the heating capacity of EAHE. It is worth noting that after the heat exchanger with the subsoil, the flowing air can no longer be heated by the building thermal mass. Hence, the source of the driving force in Mode A is the heating effect of the subsoil during the night.

Nevertheless, in Mode B, the indoor temperature varied within a larger range of 17.5− 24.9 °C (temperature difference of 7.2 °C), and the internal wall temperature fluctuated in the range 18.2−19.8 °C (temperature difference of 1.6 °C) during the two-day period. The indoor temperature was close to the outdoor temperature, as a large volume of fresh air was drawn into the indoor space (see Fig. 5). The ambient air had a direct impact on the indoor environment. In addition, the average indoor temperature was 4.0 °C higher than the outdoor temperature; however, it was slightly lower than the internal wall temperature during the early morning and night. This indicates that the heat stored in the thermal mass during high solar gains is released into the indoor air, which can partly satisfy the heating needs during the cold period.

Furthermore, in Mode C, the indoor temperature variation range was increased further from 15.4 °C to 25.0 °C (temperature difference of 9.6 °C). The low night indoor temperature and large diurnal temperature fluctuation may cause thermal discomfort. The internal wall temperature fluctuated from 16.8 °C to 18.6 °C (temperature difference of 1.8 °C) during the two-day period. Similar to that for Mode B, the indoor temperature was fairly close to the outdoor temperature owing to the direct impact of the ambient air, while the average indoor temperature was only 3.0 °C higher than the outdoor temperature and was 1.1 °C lower than the internal wall temperature during the early morning and night.

According to the previous analysis, Mode A, which uses EAHE, is superior to Modes B and C. The SCEAHE system is a passive ventilation system that preserves acceptable

indoor air quality and indoor thermal comfort.

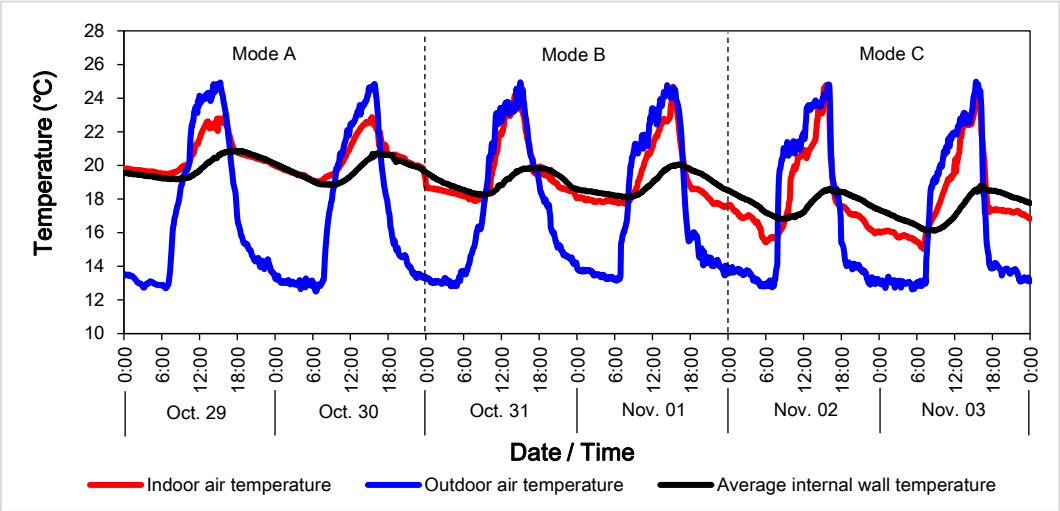

Fig. 14. Variations of average internal wall temperature, indoor air temperature and outdoor air temperature during testing period.

4. Conclusions

To confirm the positive contribution of SCEAHE system in the transition seasons, three operating modes (Modes A, B, and C) were proposed and experimentally investigated in this study. Based on the experimental results, it is showed that the SCEAHE system (operated in Mode A) has sufficient potential to preserve acceptable indoor air quality and indoor thermal comfort.

(1) Continuous and periodic natural ventilation was achieved for 24 h in the three operating modes. However, for Mode A, the driving source for nocturnal ventilation was the heating effect of the subsoil, while that for Modes B and C was the heat released from thermal mass.

(2) The average daytime and nocturnal airflow rates for Modes A, B, and C were 209 m^3/h and 139 m^3/h, 286 m^3/h and 87 m^3/h, and 340 m^3/h and 80 m^3/h, respectively. Furthermore, the average daytime airflow rate for Mode C was 18.9 % higher than that for Mode B, and 62.7 % higher than that for Mode A, while the average nocturnal airflow rate for Mode C was 8.0 % lower than that for Mode B and 42.4 % lower than that for Mode A.

(3) The outdoor air was heated and cooled in Mode A. When the inlet temperature changed from 12.5 °C to 25.0 °C, the outlet temperature varied in the range 21.4−23.0 °C. EAHE effectively elevated the fresh air temperature with a maximum increase of 8.0 °C. When the EAHE was operated under cooling conditions, the outdoor air temperature was reduced by as much as 2.5 °C. The heating and cooling capacities of the SCEAHE system were beneficial to the indoor thermal comfort. The inlet relative humidity changed from 43.8 % to 98.1 %, while the outlet relative humidity varied only between 61.9 % and 79.2 %. The nearly constant air moisture content indicated that only sensible heat transfer occurred.

(4) Relatively steady heating power (varying at approximately 350 W) was recorded during the night. Owing to the rise in the ambient air temperature, the EAHE pipe shifted from providing heating capacity to providing cooling capacity at noon and in the afternoon. The maximum cooling power was 200 W. The overall heating and cooling capacities for 24 h were 19474 kJ and 2179 kJ (approximately 9:1), respectively. The heating and cooling power is associated with the inlet air temperature of the EAHE, as the temperature of the soil surrounding the EAHE pipe is relatively steady.

(5) The soil temperature, 5 m away from the horizontal pipe inlet, at a distance of 0.15 m from the pipe surface, decreased by approximately 0.74 °C and 0.78 °C in the horizontal and vertical directions, respectively, after the two-day test. When operating the SCEAHE system, the subsoil was used as the heat sink and heat source, which partly offset the negative effect of the system on soil temperature.

(6) The indoor temperature varied within a narrow range of 19.7–22.7 °C with a temperature difference of 3.0 °C in Mode A. Nevertheless, the indoor temperature varied within a larger range of 17.5–24.9 °C with a temperature difference of 7.2 °C in Mode B. In Mode C, the indoor temperature variation range was further increased and varied from 15.4–25.0 °C (temperature difference of 9.6 °C). Low night indoor temperatures and large diurnal temperature fluctuations may cause thermal discomfort. Mode A, which uses EAHE, is superior to Modes B and C. Therefore, the SCEAHE system has the capacity to preserve acceptable indoor air quality and indoor thermal comfort.

Acknowledgments

The work described in this paper was supported by National Natural Science Foundation of China (No. 52078075, 51708054)

References

[1] Agency IE. Key World Energy Statistics. International Energy Agency (IEA) 2015.

[2] Perez-Lombard L, Ortiz J, Pout C. A review on buildings energy consumption information. Energy Build 2008; 40: 394e398.

[3] Ye W, Zhang X, Gao J, Cao G, Zhou X, Su X. Ventilated rate determinants, requirements and implementation methods for indoor pollutant control in residential buildings in China: a literature review. Science of the Total Environment 2017; 586: 696-729.

[4] Roulet CA, Heidt FD, Foradini F, et al. Real heat recovery with air handling units. Energy and Buildings 2001; 33: 495-502.

[5] Heracleous C, Michael A. Assessment of overheating risk and the impact of natural ventilation in educational buildings of Southern Europe under current and future climatic conditions. Energy 2018; 165: 1228–1239.

[6] Laverge J, Van Den Bossche N, Heijmans N, Janssens A. Energy saving potential and repercussions on indoor air quality of demand controlled residential ventilation strategies. Build. Environ. 2011; 46: 1497–1503.

[7] Omrani S, Garcia-Hansen V, Capra B, Drogemuller R. Natural ventilation in multi-storey buildings: Design process and review of evaluation tools. BUILD ENVIRON. 2017; 116: 182-194.

[8] Li Y, Liu S. Numerical study on thermal behaviors of a solar chimney incorporated with PCM. Energy and Buildings 2014; 80: 406–414.

[9] Li Y, Liu S. Experimental study on thermal performance of a solar chimney combined with PCM. Applied Energy 2014; 114: 172–178.

[10] Liu S, Li Y. An experimental study on the thermal performance of a solar chimney

without and with PCM. Renewable Energy 2015; 81: 338-346.

[11] Liu S, Li Y. Heating performance of a solar chimney combined PCM: A numerical case study. Energy and Buildings 2015; 99: 117–130.

[12] Givoni B. Climate Considerations in Building and Urban Design. Van Nostrand Reinhold, New York, 1998.

[13] Michael A, Demosthenous D, Philokyprou M. Natural ventilation for cooling in mediterranean climate: A case study in vernacular architecture of Cyprus. Energy and Buildings 2017; 144: 333–345.

[14] Cândido C, deDear RJ, Lamberts R, Bittencourt L. Air movement acceptability limits and thermal comfort in Brazil's hot humid climate zone. Building and Environment 2010; 45: 222–229.

[15] Su X, Zhang X, Gao J. Evaluation method of natural ventilation system based on thermal comfort in China. Energy and Buildings 2009; 41: 67–70.

[16] Philokyprou M, Michael A. The contribution of the courtyard to the environmental perception of residential architecture in Cyprus, in: I. Michaelides, A. Papadopoulos, A. Poullikkas (Eds.), 4th International Conference Renewable Energy Sources & Energy Efficiency, New Challenges, Nicosia, Cyprus, Proceedings, 2013, pp. 166–178.

[17] Philokyprou M, Savvides A, Michael A, Malaktou E. Examination and assessment of the environmental characteristics of vernacular rural settlements. Three case studies in Cyprus, in: M. Correia, G. Carlos, S. Sousa (Eds.), Vernacular Heritage and Earthen Architecture: Contribution to Sustainable Development, Taylor & Francis Group, London, 2014, pp. 613–618.

[18] Monghasemi N, Vadiee A. A review of solar chimney integrated systems for space heating and cooling application. Renew Sustain Energy Rev. 2018; 81: 2714–30.

[19] Khedari J, Boonsri B, Hirunlabh J. Ventilation impact of a solar chimney on indoor temperature fluctuation and air change in a school building. Energy and Buildings 2000; 32: 89–93.

[20] Zhai X, Song Z, Wang R. A review for the applications of solar chimneys in buildings. Renew. Sustain. Energy Rev. 2011; 15: 3757–3767.

[21] Brum RS, Ramalho JVA, Rodrigues MK, Rocha LAO, Isoldi LA, Santos EDD. Design evaluation of earth-air heat exchangers with multiple ducts. Renew. Energy 2019; 135: 1371-1385.

[22] Vaz J, Sattler MA, Brum RDS, Santos EDD, Isoldi LA. An experimental study on the use of Earth-Air Heat Exchangers (EAHE). Energy and Buildings 2014; 72: 122–131.

[23] Lee KH, Strand RK. The cooling and heating potential of an earth tube system in buildings. Energy and Buildings 2008; 40: 486–494.

[24] Wu H, Wang S, Zhu D. Modelling and evaluation of cooling capacity of earth–air–pipe systems. Energy Conversion and Management 2007; 48:1462–1471.

[25] Misra R, Bansal V, Agrawal GD, Mathur J, Aseri T. Transient analysis based determination of derating factor for Earth Air Tunnel Heat Exchanger in winter. Energy and Buildings 2013; 58: 76–85.

[26] Bansal V, Misra R, Agrawal GD, Mathur J. Performance analysis of earth–pipe–air heat exchanger for summer cooling. Energy and Buildings 2010; 42: 645–648.

[27] Khabbaz M, Benhamou B, Limam K, Hollmuller P, Hamdi H, Bennouna A. Experimental and numerical study of an earth-to-air heat exchanger for air cooling in a residential building in hot semi-arid climate. Energy and Buildings 2016; 125: 109–121.

[28] Li H, Ni L, Liu G, Yao Y. Performance evaluation of Earth to Air Heat Exchange (EAHE) used for indoor ventilation during winter in severe cold regions. Applied Thermal Engineering 2019; 160: 114111.

[29] Li H, Ni L, Liu G, Zhao Z, Yao Y. Feasibility study on applications of an Earth-air Heat Exchanger (EAHE) for preheating fresh air in severe cold regions. Renewable Energy 2019; 133: 1268-1284.

[30] Maerefat M, Haghighi A. Passive cooling of buildings by using integrated earth to air heat exchanger and solar chimney. Renew Energy 2010; 35: 2316–24.

[31] Li H, Yu Y, Niu F, Shafik M, Chen B. Performance of a coupled cooling system with earth-to-air heat exchanger and solar chimney. Renew Energy 2014; 62:468–77.

[32] Li Y, Long T, Bai X, Wang L, Li W, Liu S, Lu J, Cheng Y, Ye K, Huang S. An experimental investigation on the passive ventilation and cooling performance of an integrated solar chimney and earth-air heat exchanger. Renewable Energy 2021; 175: 486-500.

[33] Long T, Zheng D, Li W, Li Y, Lu J, Xie L, et al. Numerical investigation of the working mechanisms of solar chimney coupled with earth-to-air heat exchanger (SCEAHE). SOL ENERGY 2021; 230: 109-121.

[34] Ministry of Housing and Urban-Rural Development of the People's Republic of China, Design standard for energy efficiency of public buildings (GB 50189-2015), 2015.

[35] Li H, Ni L, Liu G, Zhao ZS, Yao Y. Feasibility study on applications of an Earth-air Heat Exchanger (EAHE) for preheating fresh air in severe cold regions. Renew. Energy 2019; 133: 1268-1284.

[36] Ministry of Housing and Urban-Rural Development of the People Republic of China, Standard for Energy Efficiency Test of Public Buildings (JGJ/T177-2009), China Architecture and Building Press, Beijing, China, 2010.

[37] Kirkup L, Frenkel R, An introduction to uncertainty in measurement using the GUM (guide to the expression of uncertainty in measurement), 1st ed, Cambridge: Cambridge University Press; 2006.

[38] Pátek J, Klomfar J. A computationally effective formulation of the thermodynamic properties of LiBr–H2O solutions from 273 to 500K over full composition range. International Journal of Refrigeration 2006; 29: 566-578.

[39] Benhammou M, Draoui B, Hamouda M. Improvement of the summer cooling induced by an earth-to-air heat exchanger integrated in a residential building under hot and arid climate. Appl. Energy 2017; 208: 428-445.